complexes have been interpreted on the basis of a dissociative or dissociative interchange mechanism. Accordingly, little variation has been found among the values of k_L for neutral ligands of different basicity.[39-42] On the other hand, there is a significant correlation of the rates of formation k_f with the charge type of the entering ligand.[18,44,45] This behavior has led to the suggestion that k_f (or k_L) corresponds in fact to a two-step process.[6,18,42] In the first process contributing to k_f (or k_L), the diffusion-controlled formation and dissociation of an encounter complex between $Fe(CN)_5OH_2^{3-}$ and the entering ligand (highly dependent on the charge of L) takes place (eq 12) and is followed by the second

$$Fe(CN)_5OH_2^{3-} + L^{n+} \overset{Q}{\rightleftharpoons} Fe(CN)_5OH_2^{3-}|L^{n+} \text{ rapid} \quad (12)$$

$$Fe(CN)_5OH_2^{3-}|L^{n+} \overset{k_s}{\rightleftharpoons} Fe(CN)_5L^{(3-n)-} + H_2O \text{ rate determining} \quad (13)$$

step (eq 13) where rate-determining breakage of the Fe–OH_2 bond and coordination of the incoming ligand obtain. As expected on the basis of the two-step mechanism, values of k_f ($=Qk_s$) for 3+ ligands consisting of a pentaammine moiety bound to a ligand containing an exposed, aromatic nitrogen are normally several times higher than the corresponding values measured for neutral ligands.[18,19] While this was found to be the case for Co-$(NH_3)_5Pz^{3+}$, Co-$(NH_3)_5BP^{3+}$, and Co-$(NH_3)_5BPA^{3+}$, the value of k_f for Co-$(NH_3)_5BPBD^{3+}$ falls in the range of values for the neutral ligands. In fact, there is a significant trend (Table IX) in the variation of the rates of formation with the length of the bridging ligand, with longer bridges leading to smaller values of k_f. Similarly, the rate of formation of $(NC)_5FePzRh(NH_3)_5$ has been found to be about 2 times faster than for the corresponding BP complex.[46] The reverse trend is exhibited in the reactions of $Fe(CN)_5OH_2^{3-}$ with the negatively charged ligands $Co(CN)_5L^{2-}$, the rate for Pz being about 6 times faster than that for BP.[46] An explanation of the observed trends is likely to be related to the question of dominant vs reactive ion pairs. Presumably, the dominant pairs for cationic ligands[47,48] correspond to the configurations $-CoNH_3NCFe-$, whereas the reactive ion pairs are likely to be $-CoLOH_2Fe-$. The equilibrium constants for the formation of the dominant ion pairs are rather insensitive to the identity of L, whereas the formation constants for the reactive ion pairs depend on the identity of L in a manner that reflects the Fe–Co distance, namely, the longer the ligand L, the smaller the formation constant of the reactive ion pair. For negatively charged ligands, the reverse trend obtains as anticipated for increasing distance between the negative charges in the reactive ion pairs.

Acknowledgment. This research was supported by the National Science Foundation under Grant 8502079. A.H. is indebted to Dr. Bruce Brunschwig for the calculations of the solvation energies.

Supplementary Material Available: Tables of observed rate constants (7 pages). Ordering information is given on any current masthead page.

(39) Toma, H. E.; Malin, J. M. *Inorg. Chem.* **1973**, *12*, 2080.
(40) Bradic, Z.; Pribanic, M.; Asperger, S. *J. Chem. Soc., Dalton Trans.* **1975**, 353.
(41) Szecsy, A. P.; Miller, S. S.; Haim, A. *Inorg. Chim. Acta* **1978**, *28*, 189.
(42) Toma, H. E.; Martins, J. M.; Giesbrecht, E. *J. Chem. Soc., Dalton Trans.* **1978**, 1610.
(43) Hrepic, N. V.; Malin, J. M. *Inorg. Chem.* **1979**, *18*, 409.
(44) Malin, J. M.; Ryan, D. A.; O'Halloran, T. V. *J. Am. Chem. Soc.* **1978**, *100*, 2097.
(45) Katz, N. E.; Aymonino, P. J.; Blesa, M. A.; Olabe, J. A. *Inorg. Chem.* **1978**, *17*, 556.
(46) Pfenning, K. J.; Lee, L.; Wohlers, D.; Petersen, J. D. *Inorg. Chem.* **1982**, *21*, 2477.
(47) Curtis, J. C.; Meyer, T. J. *Inorg. Chem.* **1982**, *21*, 1562.
(48) Haim, A. *Comments Inorg. Chem.* **1985**, *4*, 113.

A New Reaction Surface for Concerted Reactions: The Metal Ion Catalyzed Addition of Enolpyruvate to Pyruvate[1]

Minsek Cheong and D. L. Leussing*

Contribution from the Department of Chemistry, The Ohio State University, Columbus, Ohio 43210. *Received August 22, 1988*

Abstract: The effects of Mg^{2+} and Zn^{2+} on rates of disappearance of enzymically generated enolpyruvate along parallel ketonization and pyruvate addition paths have been measured spectrophotometrically in acetate buffers. Zn^{2+}-dependent rates of ketonization show acetate- and solvent-catalyzed pathways with rate constants of $(3.2 \pm 0.6) \times 10^4$ M^{-2} s^{-1} and $(1.3 \pm 0.4) \times 10^2$ M^{-1} s^{-1}. The former value is consistent with rate constants earlier determined[4] for Mg^{2+}-, Mn^{2+}-, and Cu^{2+}-dependent ketonization, and, in accordance with the Marcus function and as found with these earlier systems, the rate constant is in close agreement with the value predicted from the rate of decarboxylation of the corresponding metal ion complex of oxalacetate. Enolpyruvate adds to pyruvate in a metal ion dependent step to yield pyruvate dimer (**1**), according to the rate law $rate_{\text{dimer formation}} = k[M^{2+}][HEP^-][PYRU^-]$ with $k = (1.2 \pm 0.1) \times 10^4$ M^{-2} s^{-1} (Zn^{2+}) and $(4.3 \pm 0.6) \times 10^2$ M^{-2} s^{-1} (Mg^{2+}). Reaction surfaces obtained by averaging Albery and modified Guthrie surfaces were found to provide calculated rate constants that are in good agreement with the observed values using an intrinsic barrier for carbon–carbon bond formation obtained from OH^--dependent rates reported for aldol condensation and the retroaldol condensation of 3-penten-2-one. In the reaction model it is assumed that carbon–carbon bond formation is concerted with proton transfer and occurs within the coordination sphere of a metal ion–mixed ligand complex. The calculations indicate that in the transition state carbon–carbon bond formation leads proton transfer and occurs to the same extent with both metal ions. The metal ions aid in stabilizing the negative charge that appears on the pyruvate keto oxygen atom as carbon–carbon bond formation proceeds. Proton transfer from the enol oxygen atom also aids in this process, with a greater portion of the stabilization being assumed by the proton in the case of the more weakly binding Mg^{2+} ion.

How metal ions influence the reactivities of ligands that are bound to them has intrigued chemists for many years. In general, studies in this area have tended to focus on one of two broad catagories of metal ions: inert and labile. In either case ambi-

0002-7863/89/1511-2541$01.50/0

Scheme I

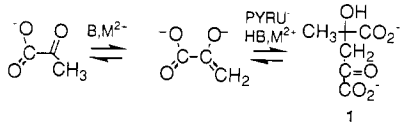

1

guities often exist as to the mode of metal ion activation. With inert metal ions it is often possible to determine the nature of slowly forming or dissociating intermediates and from these observations deduce features of the reaction path. However, slow substitution in the metal ion coordination sphere may mask the reaction of interest. Quite frequently, important information regarding the free energies of formation of species falling along the reaction pathway is absent, preventing conclusions from being drawn regarding free energy–activity relationships. In the case of labile metal ions the history of the reaction is obliterated through rapid equilibration. However, a large body of information regarding complex stabilities is available. The Marcus function,[2] eq I, defines

$$\Delta G^{\ddagger} = \Delta G^{\ddagger}_0 + \Delta G^{\circ}/2 + (\Delta G^{\circ})^2/16\Delta G^{\ddagger}_0 \qquad (I)$$

a quantitative relationship between the free energies of a reaction and its rate constant. This relationship provides a powerful tool for extracting information from observed rate constants regarding possible reaction paths. Successful applications to metal ion catalyzed enolization and decarboxylation rates have been demonstrated in earlier publications from this laboratory.[3-5] $\Delta G^{\ddagger}$ is the observed activation barrier across the *actual* rate-limiting step, $\Delta G^{\ddagger}_0$ is the intrinsic barrier for the process, and ΔG° is the thermodynamic free energy difference across the rate-limiting step.

Here we describe another application dealing with the addition of pyruvate enol to pyruvate to give pyruvate dimer, 4-methyl-4-hydroxy-2-oxoglutarate (**1**). This reaction is of interest because evidence suggests that it is strongly catalyzed by labile metal ions.[6,7] That pyruvate in the presence of heavy-metal ions readily dimerizes has been known for at least 120 years.[8-15] **1**, or its transamination product, 4-methyl-4-hydroxy-2-aminoglutarate, has been found in both plant and animal kingdoms.[16-20] The keto form is a powerful inhibitor of the Krebs cycle.[20] At least one pyruvate aldolase is known, isolated from peanut cotyledons.[16] This enzyme features an absolute requirement for divalent metal ions.

Attempts to define the rate law and obtain the rate constants for Ni^{2+}-, Cu^{2+}-, and Zn^{2+}-catalyzed pyruvate dimerization have established the presence of a two-step mechanism: general base–metal ion cocatalyzed transfer of a proton from pyruvate followed by addition of the enolate complex to a second pyruvate[6a,b,7] (Scheme I).

Scheme II

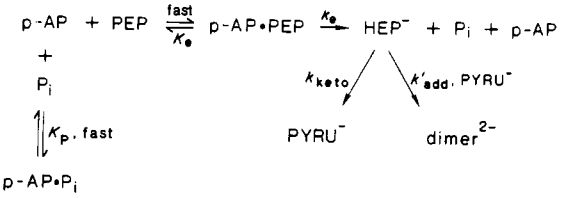

Table I. Extinction Coefficients at 240 nm

substance	ϵ_{240}	substance	ϵ_{240}
$PYRU^-$	140	H_2PEP^{-b}	422
PEP^{3-}	838	$ZnPEP^-$	540
$HPEP^{2-a}$	288	HEP^-	1490

[a] $pK_{3a} = 6.14$. [b] $pK_{2a} = 3.45$.

The slowness of the first step has frustrated efforts to gain quantitative details regarding addition. Gallo and Sable,[7] however, noted that addition appears to be much faster than is typical for aldol condensation and concluded that it is strongly catalyzed by the metal ion. Lillis[15] has demonstrated that pyruvate enol produced at a low steady state level during the decarboxylation of oxalacetate ($OXAc^{2-}$) can be trapped in the presence of Zn^{2+} to give the dimer. The yield of dimer showed a saturation effect as the concentration of pyruvate in the reaction solution was increased, suggesting that a $Zn(PYRU)^+$ complex is involved along the reaction path. It should be noted that this observation does not constitute proof that the complex is kinetically active because a saturation effect may also arise from the formation of an inactive complex in a parallel dead-end reaction.

In the present investigation pyruvate enol was generated in acetate buffers by hydrolyzing phosphoenolpyruvate (PEP) with potato acid phosphatase (p-AP).[21] Rates of disappearance of the enol along parallel addition and ketonization pathways were followed in the presence of added pyruvate and Mg^{2+} or Zn^{2+}. Addition rates resolved from the rates of disappearance were found to follow a simple rate law, first order in each of M^{2+}, pyruvate, and pyruvate enol. The rate constants are much higher than can be accounted for by a simple one-step mechanism. A reaction surface based on Scheme I and derived for a mechanism involving proton transfer concerted with carbon–carbon bond formation in a mixed ligand–metal ion complex was found to yield predicted barrier heights that are in good agreement with those observed. A similar proton transfer via mixed ligand complex formation has been concluded to give rise to fast apparent HOAc–Cu(II)-cocatalyzed ketonization of pyruvate enol.[4] The facilitation of proton transfer by way of mixed ligand complex formation may be a more important mechanistic feature of metal ion catalysis than has been appreciated to date.

Experimental Section

Experimental procedures closely followed those which had been previously described.[4] All measurements were made at 25 °C and at an ionic strength of 0.1 M (KCl). For experiments in which the influence of Zn^{2+} or Mg^{2+} on only ketonization rates of HEP^- was investigated (no added pyruvate) each kinetic run was initiated by addition of a 0.2-mL aliquot of a PEP stock solution to 1.6 mL of an acetic acid/acetate buffer containing p-AP and M^{2+}. The final concentrations were 2.0 mM PEP, 20–30 μM p-AP (corresponding to 14–20 units of *p*-nitrophenyl phosphate activity), and 0.2–0.8 mM M^{2+}. At the end of each reaction the final pH was measured. Absorbance measurements were made at 240 nm rather than at the 230-nm absorption maximum[21] of HEP^- in order to reduce background absorbance of enzyme. Addition rates were determined in similar reaction media that also contained 4.2–7.0 mM pyruvate. Immediately at the end of each reaction pyruvate in solution was determined by measuring the absorbance decrease of β-NADH at 340 nm catalyzed by lactate dehydrogenase (LDH). The analysis employed

(1) Abbreviations employed: HEP^-, pyruvate enol; EP^{2-}, pyruvate enolate; $OXAC^{2-}$, oxalacetate; PEP, phosphoenolpyruvate; ^-OAc, acetate; p-AP, white potato acid phosphatase; DSS, 2,2-dimethyl-2-silapentane-5-sulfonic acid; DAP^-, 2,3-diaminopropionate; NADH, reduced nicotinamide–adenine dinucleotide; LDH, lactate dehydrogenase.

(2) Marcus, R. A. *J. Phys. Chem.* **1968**, *72*, 891; *J. Am. Chem. Soc.* **1969**, *91*, 7224. Kresge, A. J. *Chem. Soc. Rev.* **1973**, *4*, 475.
(3) Tsai, S. J.; Leussing, D. L. *Inorg. Chem.* **1987**, *26*, 2620.
(4) Miller, B. A.; Leussing, D. L. *J. Am. Chem. Soc.* **1985**, *107*, 7146.
(5) Emly, M.; Leussing, D. L. *J. Am. Chem. Soc.* **1984**, *106*, 443.
(6) (a) Tallman, D. E.; Leussing, D. L. *J. Am. Chem. Soc.* **1969**, *91*, 6253, 6256. (b) Raghavan, N. V.; Leussing, D. L. *J. Indian Chem. Soc.* **1977**, *54*, 68.
(7) Gallo, A. A.; Sable, H. Z. *Biochim. Biophys. Acta* **1973**, *302*, 443.
(8) Finck, C. *Ann. Chem.* **1862**, *122*, 182.
(9) Wolff, L. *Ann. Chem.* **1899**, *305*, 154.
(10) Bottinger, C. *Ann. Chem.* **1881**, *208*, 122.
(11) De Jong, A. W. K. *Recl. Trav. Chim. Pays-Bas* **1901**, *20*, 81.
(12) Mulder, M. E. *Recl. Trav. Chim. Pays-Bas* **1893**, *12*, 92; **1894**, *13*, 395; **1895**, *14*, 297.
(13) Waldman, E.; Prey, V.; Jellinek, F. *Monatsh. Chem.* **1953**, *85*, 872. Prey, V.; Waldman, E.; Berbalk, H. *Monatsh. Chem.* **1955**, *86*, 408.
(14) Leussing, D. L.; Stanfield, C. *J. Am. Chem. Soc.* **1964**, *86*, 2805.
(15) Lillis, B.; Leussing, D. L. *Chem. Commun.* **1975**, 397.
(16) Shannon, L. M.; Marcus, A. *J. Biol. Chem.* **1962**, *237*, 3342.
(17) Grobbelaar, N.; Pollard, J. K.; Steward, F. C. *Nature* **1955**, *175*, 704.
(18) Linko, P.; Virtanen, A. I. *Acta Chem. Scand.* **1958**, *12*, 68.
(19) Herbert, J. D.; Coulson, R. A.; Hernandez, T. *Biochem. Biophys. Res. Commun.* **1975**, *65*, 1054.
(20) Montgomery, C. M.; Webb, J. L. *J. Biol. Chem.* **1956**, *359*, 369.
(21) Kuo, D. J.; Rose, I. A. *J. Am. Chem. Soc.* **1978**, *100*, 6288; **1982**, *104*, 3235. Kuo, D. J.; O'Connell, E. L.; Rose, I. A. *J. Am. Chem. Soc.* **1979**, *101*, 5025.

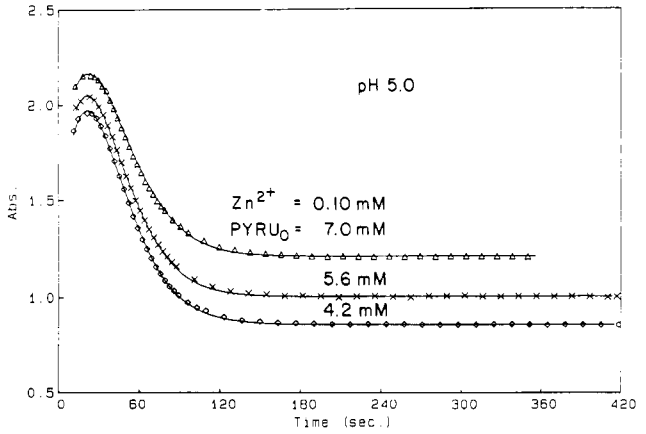

Figure 1. Absorbance–time curves for the generation and reaction of enolpyruvate in the presence of pyruvate and Zn(II). Zn(II), 0.10 mM; PEP, 2.0 mM; p-AP, 30 μM; buffer, OAc^-/HOAc total = 0.010 M, pH = 5.0; 240 nm, 0.50-cm optical path length; 25 °C, I = 0.10. The solid lines are theoretical.

10 μL of LDH (Sigma type III crystalline suspension in 2.5 M $(NH_4)_2SO_4$), 3.5 mL of 10.0 mM β-NADH (Sigma grade III in Tris buffer, pH 8.0), and 0.2 mL of reaction solution.

FT-NMR spectra (500 MHz) were obtained at the Ohio State Chemical Instrumentation Center on a Bruker AM-500 FT-NMR spectrometer. The Na salt of 2,2-dimethyl-2-silapentane-5-sulfonic acid (DSS) in H_2O was used as a reference at δ = 0. Each probe solution was prepared just before measurement.

Kinetic Analyses

Generation, ketonization, and nucleophilic attack by pyruvate enol follow the kinetics shown in Scheme II, which also includes inhibition of enzyme[4] by released phosphate.

Scheme II leads to the rate equation

$$-d(HEP^-)/dt = k'[HEP^-] - k_eK_e[\text{p-AP}][PEP]/(K_e[PEP] + 1.0 + K_P[P_i]) \quad (II)$$

where $k' = k_{keto} + k'_{add}[PYRU^-]$.

Analysis of the experimental absorbance–time curves to obtain k' was performed by using the numerical integration–nonlinear curve-fitting procedure described in ref 4. Values of the extinction coefficients at 240 nm necessary for these calculations are provided in Table I. At the low concentrations of PEP, PYRU, and divalent metal ion employed in this study, the effect of complex formation on the absorbance values could be safely ignored. The extinction coefficient of dimer was taken to be the same as that of pyruvate.[6] Small differences arising from the possible failure of this assumption have negligible effects on the evaluated rate constants. Values of K_e, K_P, and k_e were taken as determined in the earlier study.[4] Typical absorbance–time curves showing the growth and disappearance of HEP^- are shown in Figure 1. Excellent agreement is seen to have been attained between the observed data points (symbols) and the theoretical curves (solid line) calculated by numerical integration using the values of the rate parameters obtained for the optimum fit.

In the absence of added pyruvate, dimer formation is negligible and HEP^- essentially disappears only through ketonization. In the experiments in which divalent metal ion and added pyruvate were present, dimer formation becomes significant. Because pyruvate also acts as a general-base catalyst, ketonization rates obtained in the absence of added pyruvate are not a reliable measure of these rates in the dimerization studies. However, by analyzing for the amount of pyruvate present in solution at the end of the reaction, it is possible to obtain the rate constant for addition from the observed rate constant, k'.

The rate constant for dimer formation is obtained from the relationship

$$[\text{dimer}]_\infty/[PEP]_0 = k'_{add}[PYRU^-]_{av}/k' = ([PYRU^-]_0 + [PEP]_0 - [PYRU^-]_\infty)/(2[PEP]_0) \quad (III)$$

Table II. Rates of Metal Ion Catalyzed Addition of Enolpyruvate to Pyruvate[a]

Zn^{2+}

$[M^{2+}]$, mM	pH	$[PYRU^-]_0$, mM	k'_{add},[b] $M^{-1}\,s^{-1} \times 10^2$	$k'_{add}/[M^{2+}] = k_{add}$, $M^{-2}\,s^{-1} \times 10^{-4}$
0.10	5.01	4.2	0.62	1.2
0.10	5.00	5.6	0.80	1.2
0.10	5.00	7.0	1.0	1.25
0.30	5.03	4.2	1.8	1.2
0.30	5.02	5.6	2.7	1.4
0.30	5.02	7.0	2.9	1.2
0.30	4.99	4.2	1.7	1.1
0.30	4.99	5.6	2.6	1.3
0.30	4.99	7.0	2.7	1.1
0.10	4.84	4.2	0.57	1.1
0.10	4.85	5.6	0.84	1.3
0.10	4.84	7.0	0.93	1.2
0.20	4.84	4.2	1.2	1.2
0.20	4.83	5.6	1.6	1.2
0.30	4.56	4.2	1.9	1.2
0.30	4.57	5.6	2.2	1.1
0.30	4.57	7.0	2.7	1.1
0.10	4.49	4.2	0.69	1.3
0.10	4.49	5.6	0.86	1.3
0.20	4.49	4.2	1.1	1.1
0.20	4.49	5.6	1.4	1.1
0.30	4.48	4.2	1.9	1.2
0.30	4.48	5.6	2.9	1.5
				1.2 ± 0.1 av

Mg^{2+}

$[M^{2+}]$, mM	pH	$[PYRU^-]_0$, mM	k'_{add},[b] $M^{-1}\,s^{-1} \times 10^2$	$k'_{add}/[M^{2+}] = k_{add}$, $M^{-2}\,s^{-1} \times 10^{-2}$
4.0	5.08	4.2	0.89	4.3
4.0	5.08	5.6	1.1	4.2
6.0	5.06	4.2	1.2	3.8
6.0	5.06	5.6	1.5	3.8
6.0	5.06	7.0	2.0	4.2
2.0	5.06	4.2	0.51	4.9
2.0	5.06	5.6	0.69	5.2
2.0	5.06	7.0	0.83	5.2
4.0	5.04	4.2	0.81	3.9
4.0	5.04	5.6	0.98	3.7
4.0	5.04	7.0	1.5	4.7
2.0	4.91	4.2	0.50	4.8
2.0	4.91	5.6	0.70	5.3
4.0	4.90	4.2	0.76	3.7
4.0	4.90	5.6	1.3	4.9
4.0	4.90	7.0	1.5	4.7
6.0	4.91	4.2	1.1	3.5
6.0	4.91	5.6	1.5	3.8
6.0	4.90	7.0	1.8	3.8
4.0	4.71	5.6	1.0	3.8
4.0	4.72	7.0	1.7	5.3
6.0	4.69	4.2	1.0	3.2
6.0	4.69	5.6	1.5	3.8
				4.3 ± 0.6 av

[a] Absorbance measurements were made at 240 nm using 0.5-cm optical cells. In addition to the components listed above, the solutions contained 2 mM PEP and 30 μM p-AP in 0.01 M acetate/acetic acid buffer. I = 0.1 (KCl). [b] $[PYRU^-]_{avg}$ is about 1 mM greater than $[PYRU^-]_0$.

where the 0 and ∞ subscripts refer to initial and final concentrations.

Equation III can be rearranged to

$$k'_{add} = k'([PYRU^-]_0 + [PEP]_0 - [PYRU^-]_\infty)/(2[PEP]_0[PYRU^-]_{av}) \quad (IV)$$

Observed values of the product k'_{add} for Mg^{2+} and Zn^{2+} catalysis as a function of $PYRU^-$ concentration and pH are given in Table II along with calculated values of $k_{add} = k'_{add}/[M^{2+}]$.

Equilibrium Constants

The equilibrium relationships and values of the constants employed in interpreting the results are given in Table III. A number

Table III. Equilibrium Constants[a]

i	reaction *i*	log K_i	ref
1	$2CH_3COCO_2^- = \mathbf{1}$	0.78	6, 14
2	$CH_3COCO_2^- = CH_2{=}C(OH)CO_2^-$	−5.1	4
3	$CH_2{=}C(OH)CO_2^- + CH_3COCO_2^- = \mathbf{1}$	5.9	*b*
4	$CH_2{=}C(OH)CO_2^- = CH_2{=}C(O^-)CO_2^- + H^+$	−12.0	4
5	$\mathbf{1} = {}^-O_2CC(O^-)(CH_3)CH_2COCO_2^- + H^+$	−16.8	*b*
6	$CH_2{=}C(O^-)CO_2^- + CH_3COCO_2^- = {}^-O_2CC(O^-)(CH_3)CH_2COCO_2^-$	1.08	*b*
7	$CH_3C(=OH^+)CO_2^- = CH_3COCO_2^- + H^+$	≥0.0	*b*
8	${}^-O_2CC(O^-)(CH_3)CH_2C(=OH^+)CO_2^- = {}^-O_2CC(O^-)(CH_3)CH_2COCO_2^- + H^+$	>−2.5	*b*
9	$M^{2+} + CH_3COCO_2^- = [M^{2+}(CH_3COCO_2^-)]^+$	1.3 (Zn)	6
		1.1 (Mg)	4
10	$M^{2+} + \mathbf{1} = \mathbf{2}$	1.7 (Zn)	6
		1.0 (Mg)	*b*
11	$[M^{2+}(CH_2{=}C(O^-)CO_2^-)] + CH_3C(=OH^+)CO_2^- = \mathbf{2}$	12.6 (Zn)	*b*
		15.2 (Mg)	*b*
12	$M^{2+} + CH_2{=}C(O^-)CO_2^- = [M^{2+}(CH_2{=}C(O^-)CO_2^-)]$	7.0 (Zn)	*b*
		3.8 (Mg)	*b*
13	$M^{2+} + CH_2{=}C(OH)CO_2^- + CH_3COCO_2^- = \mathbf{3}$	2.8 (Zn)	*b*
		2.0 (Mg)	*b*
14	$M^{2+} + CH_2{=}C(OH)CO_2^- + CH_3COCO_2^- = \mathbf{4}$	<−10.0 (Zn)	*b*
		<−10.0 (Mg)	*b*
15a	$M^{2+} + \mathbf{5a} = \mathbf{5b}$	11.1 (Zn)	*b*
		7.0 (Mg)	*b*
15b	$M^{2+} + \mathbf{6} = \mathbf{M(6)}$	11.1 (Zn)	*b*
		7.0 (Mg)	*b*
16	$M^{2+} + CH_2{=}C(OH)CO_2^- + CH_3COCO_2^- = \mathbf{5b}$	2.7 (Zn)	*b*
		−1.4 (Mg)	*b*
17	$M^{2+} + CH_2{=}C(OH)CO_2^- + CH_3COCO_2^- = \mathbf{2}$	7.6 (Zn)	*b*
		7.0 (Mg)	*b*

[a] See Chart I for structures **2**–**5**. [b] This work.

Chart I

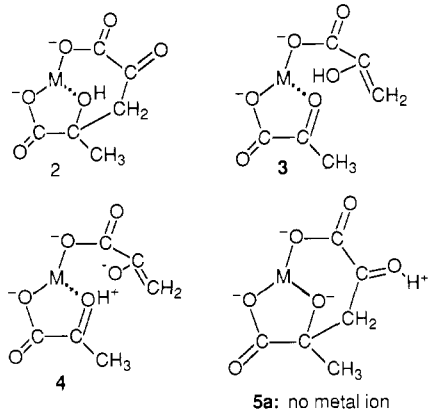

of values have been taken as reported in the literature. The derivations of other values are outlined below. pK_a values when not known were estimated by using the Taft parameters.[22]

$$\log K_3 = \log K_1 - \log K_2$$

$$-\log K_5 = 15.9 - 1.42\sum\sigma^* = 16.8$$

A value of $\sigma^*_{CH_2COCO_2} = 0.41$ was used in this calculation.[23]

$$\log K_6 = \log K_3 + \log K_5 - \log K_4$$

$$\log K_7 = -pK_{a^+HPYRU} = -pK_{a^+Hacetone} - 2.6$$

using $\rho^* = 2.4$ reported by Guthrie[24] for the ionization of RC(=OH$^+$)OH. A ρ of 2.6 is reported for the ionization of protonated acetophenones.[22] The consensus value[25] of −2.8 for $pK_{a^+Hacetone}$ places log K_7 in the vicinity of 0.0, but because Hine,[26a] Cox,[26b] and Albery[27] favor more negative values, we consider log $K_7 \geq 0.0$.

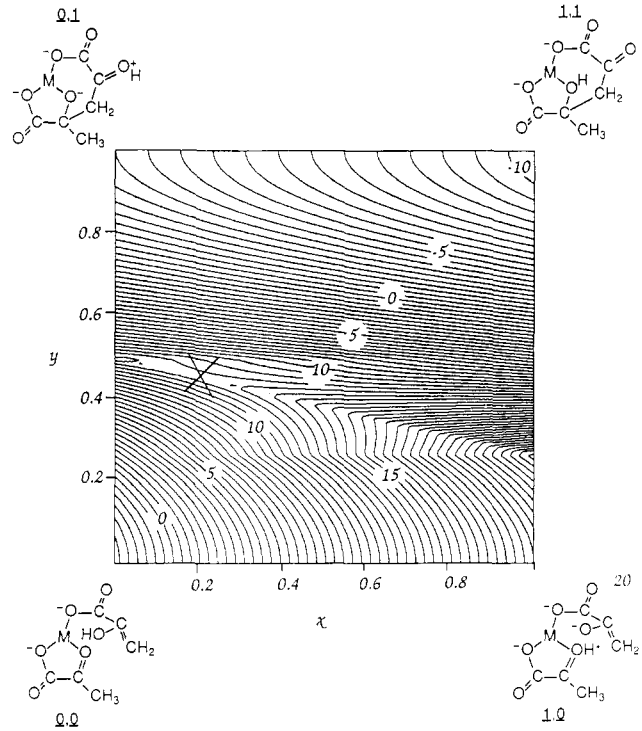

Figure 2. Contour map for Zn-mediated addition of enolpyruvate to pyruvate. Contours are drawn at 0.5-kcal intervals.

$$\log K_8 = -pK_{a^+Hacetone} - 5.3 \geq -2.4$$

using the same reasoning as used to obtain log K_7.

log K_{10} = stability constant of the metal ion–dimer complex, $M^{2+} + \mathbf{1} = \mathbf{2}$

Tallman[6a] has determined the value for the Zn^{2+} complex to be

(22) Perrin, D. D.; Dempsey, B.; Serjeant, E. P. *pK_a Prediction for Organic Acids and Bases*; Chapman and Hall: New York, 1981.
(23) Calculated from $pK_{2a}(HOXAC^-) = 4.0$.
(24) Guthrie, J. P. *J. Am. Chem. Soc.* **1978**, *100*, 5902.
(25) Stewart, R. *The Proton: Applications to Organic Chemistry*; Academic Press: New York, 1985.
(26) (a) Hine, J. *J. Am. Chem. Soc.* **1971**, *93*, 3701. (b) Cox, R. A.; Smith, C. R.; Yates, K. *Can. J. Chem.* **1979**, *57*, 2952.
(27) Albery, W. J. *J. Chem. Soc., Faraday Trans. 1* **1982**, *78*, 1579.

$10^{1.7}$ M^{-1}. From the pattern of stabilities[28] exhibited by Mg^{2+} and Zn^{2+} complexes with oxygen atom donors, we estimate the value for the Mg^{2+} complex to be $10^{1.0}$ M^{-1}.

$$\log K_{11} = \log K_7 + \log K_{17} - \log K_4 - \log K_{12}$$

$$\log K_{13} = \log K_9 + \log K_{2M(lactate)} + 0.3$$

the formation constant for forming the reactant complex **3** lying at corner 0,0 of Figure 2 from the nominal reactants, M^{2+} + HEP^- + $PYRU^-$ = **3**. The stability constant for forming the mixed-ligand complex, M(HEP)(PYRU), is estimated from the formation constant[4,6a] for $M(PYRU)^+$ and the second stepwise constant[28] for forming $M(lactate)_2$ with the application of a statistical factor of 2.0. Lactate was chosen as a surrogate for pyruvate enolate because of the similarities in the basicities of their CO_2^- groups. For Zn, $\log K_{13}$ = 1.3 + 1.2 + 0.3 = 2.8; for Mg, $\log K_{13}$ = 1.1 + 0.6 + 0.3 = 2.0. Because ligands possessing weakly binding oxygen atom donors display similar stability constants, the values are not highly sensitive to choice of ligand; e.g., if formate is chosen instead of lactate, $\log K_{13}$ = 2.5 for Zn.

$$\log K_{14} < \log K_{13} + \log K_4 - \log K_7$$

the formation constant for forming complex **4** at corner 1,0 of Figure 2 from the nominal reactants, M^{2+} + HEP^- + $PYRU^-$ = **4**. The enolate oxyanion is not bound to the metal ion but electrostatic attraction between the metal ion and the dianion and an inductive effect will cause the enol proton to be more acidic than that of the free enol. Similarly, a metal ion bound to the keto oxygen atom will substantially increase the acidity of a proton bound to this same group. Destabilization of the complex through the latter effect will dominate stabilization through the former; therefore the sum of the right-hand side of the equation determines the upper limit of the stability of complex **4**.

$$\log K_{15a} = \log K_{15b}$$

$\log K_{15a}$ is the formation constant for the reaction of **5a** with M^{2+} to yield complex **5b** at corner 0,1. This constant is not known. An estimate of the constant for binding the divalent metal ions to the ^-O_2C–CO^- group is obtained from K_{15b}, the stability constant for complex formation between M^{2+} + **6**, which is formed by the

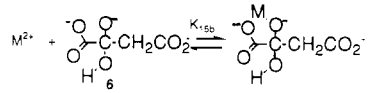

addition of OH^- to the keto carbon of $OXAC^{2-}$. The formation constants for these last complexes were estimated from the reported[3] rates of addition of OH^- to the M(OXAC) complexes. In the case of enolates[3,4] it was found that reverse calculations performed with eq I to obtain equilibrium constants from rate constants provide constants that are in excellent agreement and consistent with values obtained directly through equilibrium determinations. The measured values[3] of the rate constants for OH^- addition to $OXAC^{2-}$ are $10^{6.89}$ M^{-1} s^{-1} to Zn(OXAC) and $10^{5.46}$ M^{-1} s^{-1} to Mg(OXAC). Using a value of the equilibrium constant of $10^{-4.1}$ M^{-1} for OH^- + $OXAC^{2-}$ = **6** and taking 10.5 kcal mol^{-1} for the intrinsic barrier for OH^- attack on a keto carbon atom[3] result in values of $\log K_{15b}$ of 11.1 for Zn and 7.0 for Mg.[29] From the Taft parameters the alcohol proton of **1** is expected to exhibit a pK_a ($-\log K_5$) about 1 unit higher than the statistically corrected pK_a for OXAC hydrate (pK_{acorr} = 15.6). The effect of the positively charged substituent at the 4-position in **5a** will be to decrease this value by roughly 1.0 pK_a unit, judging from the effect of charge on the pK_a's of aminocarboxylic acids: e.g., pK_{1a}(β-alanine) = 3.5,[28] which is about 1.1 units lower than is typical for an unsubstituted aliphatic carboxylic acid at these ionic strengths. On the basis of the basicities of the oxyanions the stability constants of **5a** with the divalent metal ions are expected to lie close to those of the complexes formed by **6**. However, charge repulsion between the metal ion and the carbonyl-bound proton substituted on the 4-carbon atom of **5a** will tend to decrease the stabilities. The magnitude of this effect was estimated from contants chosen[28] for 2,3-diaminopropionate (DAP^-) interactions with Cu^{2+}. The value of pK_{3a} for HDAP is 9.40 (25 °C, I = 0.1). From entries in Table 4.2 of ref 22, the pK_a of the conjugate acid of the 2-amino group is estimated to be 1 pK_a unit lower than the pK_a of the conjugate acid of the 3-amino group; therefore, for $^+H_3NCH_2CHNH_2CO_2^-$ (**7a**) = $H_2NCH_2CHNH_2CO_2^-$ + H^+, $pK_a \approx 9.4$. The formation constant, Cu^{2+} + DAP^- = $Cu(DAP)^+$, is $10^{11.46}$ M^{-1}, and the protonation constant of the complex is $10^{4.86}$, $Cu(DAP)^+$ + H^+ = **7b**.

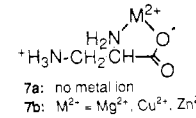

7a: no metal ion
7b: M^{2+} = Mg^{2+}, Cu^{2+}, Zn^{2+}

The log of the equilibrium constant for the reaction Cu^{2+} + **7a** = **7b** is −9.4 + 11.46 + 4.80 = 6.6. Under the same conditions the critical constant for Cu^{2+} + α-alaninate = Cu(α-alaninate) is given[28] as $10^{8.13}$ M^{-1}. This difference in stabilities suggests that charge repulsion causes a decrease roughly 1.5 log units in the stability constant of **7b**. However, a decrease of this magnitude in **5b** will be counteracted by a weak chelate effect from the interaction of the 5-CO_2^- group with the metal ion. Thus little difference between the stability constants of the **5b** complexes and those of **6** is expected.

$$\log K_{16} = \log K_3 + \log K_5 + \log K_{15a} - \log K_8 \qquad (M^{2+} + HEP^- + PYRU^- = \mathbf{5b})$$

$$\log K_{17} = \log K_3 + \log K_{10} \qquad (M^{2+} + HEP^- + PYRU^- = \mathbf{2})$$

Construction of the Combined Reaction Surface. Equation I pertains to a reaction proceeding along a single reaction coordinate, r. The free energy along the reaction path is described by two intersecting parabolas, one for the reactant state centered at r = 0 and the other for the product state centered at r = 1. Equation I gives the height of the intersection with respect to the free energy minimum of the reactants. For second-order and higher order reactions, rates are reduced to first order by forming precursor and successor complexes. This accounts for the work terms. We have followed Albery's convention[27] by taking the constant for forming a complex between two components to be 0.1 M^{-1} if one of them is neutral and 1.0 if one is an H_2O molecule. This latter choice requires that the activity on the mole fraction scale of H_2O be employed rather than its concentration; i.e., a_{water} = 1.0, so that pK_a = 0.0 for H_3O^+ and 14.0 for H_2O, before inert salt effects are taken into account.

The Fuoss equation[30] is used to correct the charge effects. Details are given elsewhere.[3,4] It is not necessary to take these preequilibria into account when reaction proceeds within the coordination sphere of a mixed-ligand complex. The stability constants of reactant and product complexes incorporate this vital information.

A concerted mechanism brings a second reaction coordinate into play so that the reaction must be viewed as proceeding along a surface, or conveniently on a contour map of such a surface.[31-38] In an investigation of metal ion effects on apparent general-acid-catalyzed enolization rates of oxalacetate, the applicability

(28) Smith, R. M.; Martell, A. M. *Critical Stability Constants*; Plenum Press: New York, 1982; Vols. 2, 5.
(29) These values are somewhat higher than those reported in ref 3, which were calculated by using an average value of the intrinsic barrier. It is now recognized that the intrinsic barrier for addition of OH^- to OXAC is 10.5 kcal.
(30) Fuoss, R. M. *J. Am. Chem. Soc.* **1958**, *80*, 5059.
(31) More-O'Ferrall, R. A. *J. Chem. Soc. B* **1970**, 274. Lewis, E. S.; Shen, C. C.; More-O'Ferrall, R. A. *J. Chem. Soc., Perkin Trans. 2* **1981**, 1084.
(32) Jencks, D. A.; Jencks, W. P. *J. Am. Chem. Soc.* **1977**, *99*, 7948.
(33) Jencks, W. P. *Chem. Rev.* **1985**, *85*, 511.
(34) Albery, W. J.; Kreevoy, M. M. *Adv. Phys. Org. Chem.* **1978**, *16*, 87.
(35) Albery, W. J. *Annu. Rev. Phys. Chem.* **1980**, *31*, 227.
(36) Kreevoy, M. M.; Lee, I.-S. H. *J. Am. Chem. Soc.* **1984**, *106*, 2550.
(37) Guthrie, J. P. *J. Am. Chem. Soc.* **1980**, *102*, 5286.
(38) Lamaty, G.; Menut, C. *Pure Appl. Chem.* **1982**, *54*, 1837.

of two reaction surfaces based on eq I had been examined. One of these surfaces was proposed by Albery[27,35] and the other was modified[3] from a scheme devised by Guthrie.[37,38] These surfaces are bounded by limiting reactions, the components of which make up the transition state for the actual reaction. Although each surface alone was found to agree well with certain of the experimental observations, neither was able to account for the entire set of results.[3] In general, the Albery surface tended to yield predicted rates that were too low while the modified Guthrie surface tended to err on the high side. More recently, we have found that a combined reaction surface, obtained by averaging the calculated free energy values obtained for both surfaces, provides predictions that are in better overall agreement with all of the experimental rate constants.[39] This combined surface is found to account for the metal ion effects observed in the present investigation.

In the present case of aldol condensation the limiting reactions are considered to involve (i) slow carbon–carbon bond formation followed by fast proton transfer

$$>C{=}O\cdots CH_2{=}C(OH)- \xrightarrow{\text{slow}} >C(O^-)CH_2C(=OH^+)- \xrightarrow{\text{fast}} >C(OH)CH_2C(=O)- \quad (18)$$

and (ii) fast proton transfer followed by slow carbon–carbon bond formation

$$>C{=}O\cdots CH_2{=}COH- \xrightarrow{\text{fast}} >C{=}OH^+\cdots CH_2{=}C(O^-)- \xrightarrow{\text{slow}} >C(OH)CH_2C(=O)- \quad (19)$$

The proton transfer occurs between two oxygen atoms and therefore is assumed to be fast (negligible barrier)[27] relative to carbon–carbon bond formation. A contour map of a surface typical of the reaction systems investigated here is shown in Figure 2, where proton transfer is depicted in the x direction and carbon–carbon bond formation in the y direction.

In order to generate free energy values falling on the Albery and modified Guthrie surfaces, estimates must be made of the free energies of the corner species. For the present reaction system these were calculated from the values of $K_{13}...K_{17}$ given in Table III for the reactions $M^{2+} + HEP^- + PYRU^- = \text{complex}_{ij}$, where i and j are the coordinates of the corners of Figure 2. The Albery surface is generated by calculating free energy–reaction coordinate profiles at discrete intervals along the abscissa. These profiles are comprised of a family of intersecting parabolas lying parallel to the ordinate. The equations used to construct the parabolas are

$$\Delta G_{xy} = 4(\Delta G^{\ddagger}_0)y^2 + (1-x)\Delta G^{\circ}_{00} + x\Delta G^{\circ}_{10} \quad \text{(reactant side of transition state, } y \le y^{\ddagger}) \quad \text{(V)}$$

and

$$\Delta G_{xy} = 4\Delta G^{\ddagger}_0(y-1)^2 + (1-x)\Delta G^{\circ}_{01} + x\Delta G^{\circ}_{11} \quad \text{(product side of transition state, } y > y^{\ddagger}) \quad \text{(VI)}$$

The Albery surface displays a ridge that connects the two transition states lying on the left-hand ($x = 0$) and right-hand ($x = 1$) vertical axes. The points lying along this ridge comprise the possible transition states. For a given value of the x coordinate the corresponding value of the y coordinate on the ridge is given by the equation

$$y_{\text{ridge}} = (4\Delta G^{\ddagger}_0 + \Delta G^{\circ}_x)/8\Delta G^{\ddagger}_0 \quad \text{(VII)}$$

where

$$\Delta G^{\circ}_x = x(\Delta G^{\circ}_{11} - \Delta G^{\circ}_{10}) + (1-x)(\Delta G^{\circ}_{01} - \Delta G^{\circ}_{00}) \quad \text{(VIII)}$$

Free energies located along the Albery ridge for given values of x are calculated by using eq VIII, VII, and V.

The modified Guthrie surface[4,37] is constructed by calculating free energy–reaction coordinate profiles only for $x = 0$ and 1, the left-hand and right-hand axes, and linearly interpolating in the horizontal direction at intervals along the y axis

$$\Delta G_{xy} = (1-x)\Delta G_{0y} + x\Delta G_{1y} \quad \text{(IX)}$$

The appropriate values of ΔG_{0y} and ΔG_{1y} are obtained from eq V and VI for $x = 0$ and 1.

Under the appropriate conditions[37] this surface is characterized by a "catalytic" cleft that is located between the two transition states lying on the boundaries defined by $x = 0$ and 1.

Because the Albery surface constitutes a vertical interpolation along the reaction surface and the Guthric surface a horizontal one, it seems reasonable to expect that the values of the interior points are more accurately determined by all four boundaries rather than only two. Combining the two surfaces into a single one through averaging generates a surface having a pass (transition state) that falls in the vicinity of the intersection of the Albery ridge and the Guthrie catalytic cleft. We approximate the location of the transition state by searching for a free energy minimum along the Albery ridge using small (≤ 0.01) increments of x and eq VIII, VII, and V.

A value of $\Delta G^{\ddagger}_0$ is required for the construction of the reaction surface. One estimate was obtained from rate studies reported by Gruen and McTigue[40] for OH^--catalyzed aldol condensation of acetaldehyde. These authors found a rate law corresponding to the reaction sequence

$$CH_3CHO + OH^- \underset{k_{-20a}}{\overset{k_{20a}}{\rightleftharpoons}} CH_2{=}CHO^- + H_2O \quad \text{(20a)}$$

$$CH_2{=}CHO^- + CH_3CHO \underset{k_{-20b}}{\overset{k_{20b}}{\rightleftharpoons}} CH_3CH(O^-)CH_2CHO \quad \text{(20b)}$$

$$CH_3CH(O^-)CH_2CHO \overset{H_2O,\ \text{fast}}{\rightleftharpoons} CH_3CH(OH)CH_2CHO + OH^- \quad \text{(20c)}$$

$$K_{20a} = k_{20a}/k_{-20a}, \qquad K_{20b} = k_{20b}/k_{-20b}$$

Values of 0.15 M^{-1} s^{-1} and 1.3 M^{-1} were determined for k_{20a} and the ratio k_{-20a}/k_{20b}. The enol/keto ratio of acetaldehyde and the pK_a of the enol have been determined.[41] The equilibrium constant for aldol condensation has been found[42] to be 400 M^{-1}. From these values $\Delta G^{\ddagger}_0$ for carbon–carbon bond formation in the addition of the enolate of pyruvate to the keto carbon of pyruvate is calculated to be 15.6–15.8 kcal mol^{-1}. A close-lying value of 15.7 kcal mol^{-1} was similarly calculated from rates reported by Guthrie[43] for the retroaldol condensation of 3-penten-2-one

$$CH_3CH{=}CHC(=O)CH_3 \overset{H_2O}{\rightleftharpoons} CH_3CH(OH)CH_2C(=O)CH_3 \overset{OH^-}{\rightleftharpoons} CH_3CHO + CH_3COCH_3 \quad (21)$$

The details of these calculations are presented in the Appendix.

It is of interest to note that the intrinsic barrier for carbon–carbon bond formation in the addition of enolate to carbonyl carbon occupies an intermediate position between the barriers found for carbon–carbon bond formation in $OXAC^{2-}$ decarboxylation (18 kcal)[4] and carbon–hydrogen ion dissociation in enolization (13.7 kcal).[3] This spread of 4 kcal in the $\Delta G^{\ddagger}_0$ values represents approximately a 1000-fold variation in the inherent rate constants.

Results and Discussion

Ketonization. Zn^{2+}-dependent ketonization rates, calculated from measured rates of HEP^- disappearance in the absence of added pyruvate, were found to be first order in each of Zn^{2+}, HEP^-, and acetate, in agreement with the results earlier reported by Miller[4] for Mg^{2+}-, Mn^{2+}-, and Cu^{2+}-catalyzed HEP^- ketonization. In addition, with Zn^{2+} a solvent-catalyzed route is observed. The results are $k_{\text{keto,Zn,OAc}} = (3.2 \pm 0.6) \times 10^4$ M^{-2} s^{-1} and $k_{\text{keto,Zn,solvent}} = (1.3 \pm 0.4) \times 10^2$ M^{-1} s^{-1}. These rate terms

(39) To be published.

(40) Gruen, L. C.; McTigue, P. T. *Aust. J. Chem.* **1964**, *17*, 953.
(41) Chiang, Y.; Hojatti, M.; Keeffe, J. R.; Kresge, A. J.; Schepp, N. P.; Wirz, J. *J. Am. Chem. Soc.* **1987**, *109*, 4000.
(42) Guthrie, J. P. *Can. J. Chem.* **1974**, *52*, 2037.
(43) Guthrie, J. P. *Can. J. Chem.* **1981**, *59*, 45.

do not arise from a true general-base-catalyzed reaction of the enol complex. The rate-limiting step actually involves the kinetically equivalent transfer of a proton from the conjugate acid of the apparent base catalyst to the methylene carbon of the enolate complex.

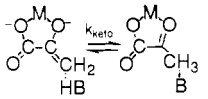

In the earlier work[4] the rather remarkable result had been demonstrated that metal ion–apparent general base cocatalyzed ketonization rates of HEP^- may be predicted with exceptionally good accuracy from the decarboxylation rates of M(OXAC) complexes. This relationship is based on the fact that both reactions involve pyruvate enolate complexes.

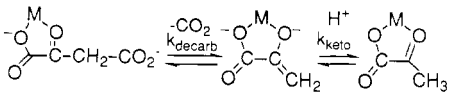

Equation I implies that the effect of the stability of an M(EP) complex on one of the reaction rates must be reflected by an inverse effect on the other. For example, the higher is the stability of the intermediate M(EP) complex, the faster is the rate of $OXAC^{2-}$ decarboxylation and the slower is the rate of proton transfer to carbon in the ketonization of the enolate. The relationship is actually quantitative. If the rates and equilibrium constants for both reactions in the *absence* of metal ions are known (which allows the two intrinsic barriers to be evaluated), the determination of the rate constant for a metal ion dependent pathway for one of the reactions enables the rate constant to be calculated for the corresponding metal ion dependent path for the other reaction. The additional data required are the stability constants of the $OXAC^{2-}$ and $PYRU^-$ complexes.[4] Our results for Zn(II)-catalyzed HEP^- ketonization lend further support to this relationship. The experimental value of 4.5 for log $k_{keto,Zn-OAc}$ is in excellent agreement with a value of 4.6 calculated from the decarboxylation rate constant of 0.045 s^{-1} determined for Zn(OXAC).[44] The stability constant for $Zn^{2+} + EP^{2-} = Zn(EP)$ is calculated to be $10^{7.0}$ M^{-1} by performing the reverse calculation using eq I and 13.7 kcal mol^{-1} for $\Delta G^{\ddagger}_{0,enolization}$. This result is in line with the earlier[4] values determined for the stabilities of the EP^{2-} complexes of Mg^{2+}, Mn^{2+}, and Cu^{2+}.

If complexing metal ions actually inhibit proton transfer to enolate carbon, how then does their presence increase the ketonization rate of pyruvate enol? The answer lies in the fact that enolates undergo carbon protonation at rates that are about 10^6–10^9 times as fast as enols.[45] Metal ions, by forming stable pyruvate enolate complexes, convert the enol to a much more reactive form, $M^{2+} + HEP^- \rightleftharpoons M(EP) + H^+$ (K_{pre}, fast), $M(EP) + HB \rightarrow M(PYRU)^+ + B$ ($k_{transfer}$, slow). The experimental third-order rate constant is determined by the product $K_{pre}k_{transfer}$. K_{pre} increases according to the first power of the stability constant of the M(EP) complex but because the quadratic term in eq I is usually small, $k_{transfer}$ decreases approximately according to the one-half power of this stability constant. The net result is that the product of these two constants increases according to the one-half power of the stability constant of the M(EP) complex, so that the more strongly binding is the metal ion to the enolate, the faster is the rate of enolization, as long as metal ion concentrations lie below the saturation value. This prediction of a square root dependency of rate on stability constant has been experimentally verified.[4]

Dimerization. The equilibrium constant for the addition of one pyruvate to another to form **1** has a modest value of 6 M^{-1} (K_1),[6a] but a higher value of $10^{5.9}$ M^{-1} is calculated for the reaction of the considerably more active pyruvate enol with pyruvate (K_3). The importance of neutralizing the negative charge on the oxygen atom at the 4-position of the adduct is underscored by the fact that the addition constant is only $10^{1.08}$ M^{-1} for the reaction of the enolate with pyruvate to give the deprotonated adduct (K_6). This inherent instability of the deprotonated adduct has important overtones with respect to the kinetics and is a major factor in determining the catalytic influence of metal ions on the rates.

^1H NMR provides evidence that the divalent metal ion must be present in the reaction solution in order for detectable levels of dimer to be formed in acetate buffers at the low concentrations of added pyruvate employed. The presence of **1** is readily discerned through a sharp CH_3 resonance at δ = 1.38 and a CH_2 multiplet centered at 3.35 ppm. This last band shows an AB pattern owing to the influence of the adjacent chiral center (J_{AB} = 17.6 Hz). A solution in 50% H_2O/D_2O initially containing 30 μM p-AP, 2 mM PEP, and 5 mM $PYRU^-$ at pH 4.5 shows neither PEP resonances[46] nor dimer bands in a spectrum collected at 10 min after mixing. However, when a reaction solution having the same composition is also made 0.5 mM in Zn^{2+}, peaks characteristic of **1** at 1.38 and 3.35 ppm are apparent in the 10-min spectrum. In the absence of PEP and p-AP, pyruvate dimer peaks are not observed in solutions at these Zn^{2+} and pyruvate concentrations even after the solutions have been allowed to stand for an hour.

Rates of dimer formation correspond to a rate law that is first order in each of metal ion, $PYRU^-$, and HEP^-. Values of $k_{add}/[M^{2+}][PYRU^-]_{av}$ are seen in Table II to be constant, averaging 1.2 (1) × 10^4 M^{-2} s^{-1} for Zn^{2+} catalysis and 4.3 (6) × 10^2 M^{-2} s^{-1} for Mg^{2+} catalysis. $[PYRU^-]_{av}$ is the average of the initial and final concentrations of $PYRU^-$ in a reaction mixture.

In general-base-catalyzed enolization metal ions promote rates by substantially stabilizing the enolate product with respect to the keto reactant;[3] however, in the present case the product complexes are only slightly more stable than the reactant complexes. Tallman[6a] has determined the constant for binding Zn^{2+} to **1** to be $10^{1.7}$ M^{-1}. The formation constant of $Zn(HEP)^+$ is estimated[4] to lie in the vicinity of $10^{1.0}$ M^{-1}; therefore differences between ground-state interactions of reactant HEP^- and **1** with the metal ion exert little influence on the activation barrier for addition. In contrast, high stabilities of the deprotonated adduct complexes at corner 0,1 of Figure 2 relative to the lower stabilities of the $M(HEP)^+$ complexes are capable of providing sufficient driving force to substantially lower the activation barrier. The stability constants of the adduct complexes, **5b**, are $\approx 10^{11.1}$ for Zn^{2+} and $10^{7.0}$ for Mg^{2+} while those for the $M(HEP)^+$ are $\approx 10^{1.0}$ M^{-1} for both metal ions.

Earlier[6,14] it had been proposed that Zn^{2+}-mediated pyruvate dimerization in acetate buffers occurs via a mixed-ligand complex involving chelated pyruvate enolate and *monodentately* bound pyruvate (addition is sterically inhibited if both ligands are chelated to the metal ion). However, this mechanism cannot be correct because the present investigation shows that under the pH conditions present in acetate buffers a proton is also present in the transition state. By assuming a model in which the pyruvate is chelated and pyruvate enol is monodentately bound to the metal ion, as shown in **3**, it is found possible to obtain calculated rate constants that are in excellent agreement with those observed. In **3** the metal ion is in place to stabilize the negative charge that develops on the keto oxygen atom of pyruvate as carbon–carbon bond formation proceeds. This process is further aided by a concerted proton transfer from the enol oxygen atom to the keto oxygen atom. Molecular models show that in the mixed-ligand complex the ligands are able to attain a configuration in which the reacting carbon atoms are brought into contact with the enol proton lying in close proximity to the keto oxygen atom.

For the combined reaction surface for this proposed mechanism, shown in Figure 2, the free energy of the nominal reactants, M^{2+}, HEP^-, and $PYRU^-$, is taken as the reference point at 0 kcal. These species are brought together to form the reactant mixed-ligand

(44) Emly, M. Ph.D. Thesis, The Ohio State University, 1979; Leussing, D. L. "The Enzymatic and Non-Enzymatic Decarboxylation of Oxalacetate". In *Advances in Inorganic Biochemistry*; Eichhorn, G. L., Marzilli, L. G., Eds.; Elsevier Biomedical: New York, 1982; Chapter 5.

(45) Chiang, Y.; Kresge, A. J.; Santaballa, J. A.; Wirz, J. *J. Am. Chem. Soc.* **1988**, *110*, 5506.

(46) Cohn, M.; Pearson, J. E.; O'Connell, E. L.; Rose, I. A. *J. Am. Chem. Soc.* **1970**, *92*, 4095.

Table IV. Dependence of the Logarithms of the Predicted Rate Constants and the Location of the Transition State on the Free Energies of the Corner Species ($\Delta G^{\ddagger}_0$ = 15.6 kcal mol^{-1})

pt	ΔG^0_{00}	ΔG^0_{10}	ΔG^0_{01}	ΔG^0_{11}	$x^{\ddagger}$	$y^{\ddagger}$	log k_{calcd}[b]
			Zn^{2+} (log k_{obsd} = 4.06[b])				
1	−3.8	13.0	−4.0	−10.4	0.23	0.46	4.72
2	−3.8	20.0	−4.0	−10.4	0.17	0.46	4.57
3	−3.8	27.0	−4.0	−10.4	0.13	0.46	4.48
4	−3.8	20.0	−3.0	−10.4	0.20	0.46	4.35
5[a]	−3.8	20.0	−4.0	−10.4	0.17	0.46	4.21
6	−3.8	20.0	−4.0	−9.4	0.15	0.46	4.47
7	−2.8	20.0	−4.0	−10.4	0.17	0.45	4.19
			Mg^{2+} (log k_{obsd} = 2.63[b])				
8	−2.7	13.0	1.9	−9.5	0.38	0.46	3.26
9	−2.7	20.0	1.9	−9.5	0.29	0.46	2.90
10	−2.7	27.0	1.9	−9.5	0.24	0.46	2.67
11	−2.7	20.0	1.9	−8.5	0.28	0.46	2.73
12	−1.7	20.0	1.9	−9.5	0.30	0.45	2.54
13[a]	−2.7	20.0	1.9	−9.5	0.30	0.46	2.54
14	−2.7	20.0	2.9	−9.5	0.31	0.46	2.75
			No Metal Ion				
15[d]	1.8	18.2	11.5	−8.0	0.49	0.44	0.12[c]
16[e]	1.8	22.3	15.6	−8.0	0.48	0.44	−0.64[c]

[a] $\Delta G^{\ddagger}_0$ = 16.1 kcal. [b] Third-order rate constant. [c] Second-order rate constant. [d] pK_{a^+HPYRU} = 0.0. [e] pK_{a^+HPYRU} = −3.0.

complex **3** which lies at the lower left-hand corner, coordinate 0,0. One limiting pathway involves the fast transfer of the enol proton to the keto oxygen atom to generate the species **4** lying at corner 1,0. This complex undergoes carbon–carbon bond formation in a slow step to give the product **2** at corner 1,1. The other limiting path assumes slow carbon–carbon bond formation prior to fast proton transfer. **5b** formed at corner 0,1 along this latter route undergoes fast tautomerization to produce product at corner 1,1.

The surface shown in Figure 2 for Zn^{2+} catalysis was calculated by taking $\Delta G^{\ddagger}_0$ = 16.0, ΔG°_{00} = 3.3, ΔG°_{01} = 4.0, ΔG°_{11} = 10.4, and ΔG°_{10} = 20.0 kcal mol^{-1}. The transition state, indicated by X, lies at $x^{\ddagger}$ = 0.26 and $y^{\ddagger}$ = 0.49 with 11.5 ≤ $\Delta G^{\ddagger}_{calcd}$ ≤ 12.0 kcal. The predicted height of the barrier is close in value to the experimental result, $\Delta G^{\ddagger}_{obsd}$ = 11.86 kcal.

The free energies of the reactant and product are known with reasonable accuracy, but those for the off-diagonal species at corners 1,0 and 0,1 are more uncertain, particularly that of the protonated complex **4** lying at corner 1,0. Fortunately, the results are not highly sensitive to these latter free energies. The calculated effects of varying the free energies on the predicted rate constants are shown in Table IV. If the metal ion in **4** exerted no influence on the basicities of the enolate and keto oxygen atoms, ΔG°_{10} would be about 13 kcal, the value taken in the calculations for lines 1 (Zn) and 8 (Mg) of Table IV. The binding of the divalent metal ion as shown in structure **4** will cause the enolate to become more stable and the protonated >C=O group to become less stable, with the latter effect dominating. A net destabilization of about 10 pK_a units between the basicities of these groups represents an increase in the value of ΔG°_{10} to about 27 kcal. This is the value assumed for ΔG°_{10} in calculating lines 3 and 10 of Table IV and it is seen that log k_{calcd} only decreases from about 4.7 to 4.5 in the case of Zn and from about 3.3 to 2.7 in the case of Mg.

In calculating the effect of varying the free energies at the remaining corners of the reaction surface, an intermediate value of ΔG°_{10} was assumed (lines 2 and 9, Table IV). With reference to these data, it is seen that a change in the free energy at corner 0,1 by 1.0 kcal translates to a change of log k_{calcd} by about 0.2 unit with both metal ions. A change of the same magnitude in the estimated free energies of the product at corner 1,1 changes the calculated rate constants by only 0.1 to 0.2 log unit. log k_{calcd} decreases by 0.3–0.4 unit with each metal ion for a 1-kcal increase in ΔG°_{00}. The value of the intrinsic barrier has the largest effect on log k_{calcd} which increases by about 0.7–0.9 unit for each kcal increase in $\Delta G^{\ddagger}_0$. Within fairly generous allowances in the free energies of the corner species, the values of log k_{calcd} are seen to be in gratifyingly good agreement with the observed values of 4.1 (Zn) and 2.6 (Mg).

The value of $x^{\ddagger}$ at the transition state is a measure of the degree of proton transfer from enol to the pyruvate keto oxygen atom, and $y^{\ddagger}$ is a measure of the degree of carbon–carbon bond formation.[32,33] The higher value of $y^{\ddagger}$ indicates that bond formation leads proton transfer, implying that the metal ion functions not only to bring the reactants together but also plays a substantial role in stabilizing the negative charge developing on the pyruvate oxygen atom. The saturation effect observed by Lillis[15] in the enol-trapping experiments lends support to the proposed formation of a kinetically activated Zn^{2+}–pyruvate–enol complex, such as **3**.

In accordance with the Marcus equation, the weaker stabilities of Mg^{2+} complexes relative to Zn^{2+} complexes accounts for the lower catalytic rates observed with Mg^{2+}. Particularly important in determining the rate difference are the relative stabilities of the complexes formed at corner 0,1. The value of $y^{\ddagger} \approx 0.45$–0.46 for Mg^{2+} catalysis is identical with that obtained for Zn^{2+}, indicating that the nature of the metal ion has little influence on the extent of carbon–carbon bond formation in the transition state. However, values of $x^{\ddagger}$ lying in the range 0.24–0.38 for Mg^{2+} and 0.13–0.23 for Zn^{2+} indicate that proton transfer assumes a greater degree of transition-state stabilization with Mg^{2+} than is found with Zn^{2+}. This difference in transition-state structure is consistent with the weaker binding of Mg^{2+}, particularly at corner 0,1.

It is further instructive to examine the values predicted for the rate constants and transition-state locations for the addition of HEP^- to $PYRU^-$ in the absence of complexing metal ions. Line 15, Table IV, shows the results that are obtained assuming that pK_{a^+HPYRU} (−log K_7) lies at the upper limit (0.0) and the reactive groups of the enol and ketone in the precursor complex are brought into juxtaposition just as they are in the mixed-ligand complexes. The value of 1.8 kcal mol^{-1} taken for ΔG° at corner 0,0 has been calculated assuming a precursor complex formed from two species, each bearing a charge of −1 (K_{pre} = 0.048^{-1}). The value of 1.3 M^{-1} s^{-1} that is obtained for the rate constant is large enough that under the reaction conditions described in Table II a metal ion independent component should be discerned. This independence on metal ion is not evident in the results. A value of $pK_{a^+HPYRU} \approx -3.0$ is compatible with $pK_{a^+acetone}$ = −5.37 reported by Cox.[26b] The predicted rate constant of 0.23 M^{-1} s^{-1} (line 16, Table IV) is more in line with the observations, but a tacit assumption that the statistical effect for bringing the two sets of reacting groups together in an HEP^-···$PYRU^-$ cage complex is the same as bringing them together in the metal ion complex prevents drawing a firm conclusion regarding the appropriate value of pK_{a^+HPYRU} to be employed in these calculations. It would seem that in the former case the chances of attaining the proper alignment of the two sets of reactive groups is less than when their carboxylate groups are anchored to the same metal ion. In this context the choice by Albery of 0.1 M^{-1} for the formation constant of a precursor or successor complex comprised of at least one neutral species is consistent with the reactivities observed for metal ion complexes. An implied statistical factor in proceeding from this dominant state to the actual reaction configuration seems to be the same for the metal ion complexes as with the single-coordinate addition of the acetaldehyde enolate to acetaldehyde.

Regarding the transition state, it is seen in Table IV that in the absence of the metal ion the degree of carbon–carbon bond formation is slightly lower than in its presence, but the degree of proton transfer is substantially higher, as is expected. The degree of carbon–carbon bond formation is determined mainly from the free energy difference, $\Delta G^{\circ}_{11} - \Delta G^{\circ}_{00}$, which in this case is not greatly influenced by the metal ion because of a relatively small difference in the reactant and product stability constants. However, the metal ion has a very substantial influence on the difference, $\Delta G^{\circ}_{01} - \Delta G^{\circ}_{10}$, which affects the position of the proton in the transition state.

By taking a concerted pathway the reaction system avoids unfavorable preequilibrium steps. In order to illustrate this point

it is instructive to predict the rate constant for another plausible pathway that is consistent with the observed rate law. This route involves the addition of the metal ion activated enolate complex to carbonyl protonated pyruvate

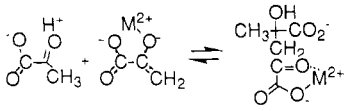

One rationale for considering this pathway is the extensive use of metal ion activated enolates in organic synthesis. Another is the finding by Cox[47] that in sulfuric acid solutions aldol condensation proceeds via general-base catalysis by H_2O of enol attack on protonated acetaldehyde.

If pK_{a^+HPYRU} is taken as 0.0, log K_{11} = 12.6, leading to a predicted second-order rate constant of $10^{5.8}$ M^{-1} s^{-1}. Conversion to the third-order rate constant expressed in terms of the concentrations of the nominal reactants, Zn^{2+}, HEP^-, and $PYRU^-$, results in a value of $10^{0.8}$ M^{-2} s^{-1}, which is about 4 orders of magnitude smaller than the observed value. Although, the second-order rate constant shows that reaction of the activated species Zn(EP) and $CH_3C(=OH^+)CO_2^-$ is rapid, the preequilibrium expenditure of free energy required to form these reactants from the nominal reactants is too unfavorable to allow this pathway to be competitive with the concerted route, in which the metal ion plays a richer role in reducing the activation barrier.

In conclusion, the model reaction surface proposed here provides excellent quantitative agreement between observed and calculated rate constants using an intrinsic barrier obtained from a metal ion independent rate of aldol condensation and independently derived free energies of formation of the metal ion complexes that lie at the corners of the surface. A plausible picture of the action of the metal ion on the reaction path has been drawn: the metal ion brings the reactants together as a rather loose complex in which concerted carbon–carbon bond formation and proton transfer can readily occur; the metal ion and the in-flight proton act together to stabilize the adduct by neutralizing negative charge that develops on the keto oxygen atom as carbon–carbon bond formation progresses; the more weakly binding is the metal ion, the greater is the degree of stabilization provided by the proton.

In effect, the metal ion submits the reaction surface to a major perturbation. By significantly raising the free energy of one of the off-diagonal species (that at corner 1,0 in the present example) and significantly lowering the free energy of the other off-diagonal species (at corner 0,1), the surface is subjected to a *quasi*-rotation about the main diagonal. The accompanying decrease in the height of the activation barrier with respect to the free energy of nominal reactants is one source of the catalytic effect. Another contributing factor is the facile ability to form the preequilibrium reactant complex.

In a number of recent publications dealing with concerted reactions, the reaction surface has been viewed in the context of a hyperbolic paraboloid, a surface that possesses a saddle point.[32,33,48,49] The reaction surface described here provides an alternate approach for treating concerted reactions. A major advantage is the ability to use an independently derived intrinsic activation barrier in the calculations. Further studies on the validity of this approach and comparisons with the properties of surfaces based upon the hyperbolic paraboloid are in progress.

Appendix

A. Evaluation of $\Delta G^{\ddagger}_0$ for Aldol Condensation from the Rate Constant for OH^--Catalyzed Aldol Condensation. The value of k_{20b} for reaction 20b can be calculated from available information. Guthrie[42] has determined K_{aldol} for $2CH_3CHO = CH_3CH(OH)CH_2CHO$ to be 400 M^{-1}. The enol/keto ratio of acetaldehyde[41] is 5.89×10^{-7} and the pK_a of vinyl alcohol[41] is 10.5. Using the Taft parameters,[22] one calculates the pK_a of the alcohol proton of aldol to be 15.0. Taking K_w for the autoprotolysis of water to be $10^{-13.7}$ for 25 °C, I = 0.1, the equilibrium constants for reactions 20a–c are evaluated to be $K_{20a} = 5.89 \times 10^{-7} \times 10^{-10.5+13.7} = 9.3 \times 10^{-4}$ M^{-1}, $K_{20c} = 10^{+15.0-13.7}$ M = 20 M, and $K_{20b} = 400/K_{20a}K_{20c} = 2.15 \times 10^4$ M^{-1}.

The value of k_{-20a} has been determined to be 882 M^{-1} s^{-1}; therefore, $k_{20b} = 882/1.3 = 6.8 \times 10^2$ M^{-1} s^{-1}.

The constant for forming the precursor complex prior to addition in reaction 20b is 0.1 M^{-1}, $CH_2CH(O^-) + CH_3CHO = CH_2CH(O^-)\cdots CH_3CHO$. Since $K_{20b} = K_{precursor} \times K_{20b,rate\ limiting}$, $K_{20b,rate\ limiting} = 2.15 \times 10^4/0.1 = 2.15 \times 10^5$. The value of $k_{20b,rate\ limiting}$ is $6.8 \times 10^2/0.1 = 6.8 \times 10^3$ s^{-1}. Pertaining to eq I, $\Delta G^{\ddagger} = -1.36 \log (6.8 \times 10^3) + 17.4 = 12.17$ kcal, and $\Delta G^{\circ} = -7.27$ kcal. Solving for $\Delta G^{\ddagger}_0$ gives 15.6 kcal mol^{-1}.

Alternatively, using an enol/keto ratio[53] of 2.7×10^{-7} and an estimate of 11.1 for the pK_a of vinyl alcohol[54] results in $\Delta G^{\ddagger}_0$ = 15.8 kcal mol^{-1}.

B. Evaluation of $\Delta G^{\ddagger}_0$ from the OH^--Catalyzed Rate of Dissociation of 4-Hydroxy-2-oxopentene. Guthrie[43] has determined the rate constant for the retroaldol condensation of the hydrate in reaction 21 to be 3.4×10^{-4} M^{-1} s^{-1}. This reaction proceeds in three steps

$$CH_3CH(OH)CH_2C(=O)CH_3 + OH^- = CH_3CH(O^-)CH_2C(=O)CH_3 + H_2O \text{ (fast)} \quad (1A)$$

$$CH_3CH(O^-)CH_2C(=O)CH_3 \rightarrow CH_3CHO + CH_2=C(O^-)CH_3 \text{ (slow)} \quad (2A)$$

$$CH_2=C(O^-)CH_3 + H_2O = CH_3COCH_3 + OH^- \text{ (fast)} \quad (3A)$$

Kresge[50] has determined pK_a(acetone) = 19.16 (keto to enolate) and the rate constant for the reverse of reaction 3A to be 0.220 M^{-1} s^{-1} (25 °C, I = 0.1). Thus the equilibrium constant for reaction 3A is $K_{3A} = 10^{-13.7+19.16} = 10^{5.46}$ M, and the rate constant in the forward direction is 6.3×10^4 s^{-1}.

Structure–reactivity relationships deduced by Sander and Jencks[51] and Guthrie[52] for carbonyl addition reactions allow the addition constant for $CH_3COCH_3 + CH_3CHO = CH_3CH(OH)CH_2C(=O)CH_3$ to be estimated as 19 M^{-1}. The pK_a of the alcohol proton is estimated[22] to be 15.0.

If $K_{3A} = 10^{5.46}$ and $K_{1A} = 10^{13.7-15.0} = 0.05$ M^{-1}, then $K_{2A} = 3.7 \times 10^{-6}$ M from the relationship $1/19 = K_{1A}K_{2A}K_{3A}$. Likewise, $k_{2A} = 3.4 \times 10^{-4}/K_{1A} = 6.8 \times 10^{-3}$ s^{-1}.

Because $K_{2A} = K_{rate\ limiting}/K_{successor}$ and $K_{successor}$ = 0.1 M^{-1}, $K_{rate\ limiting} = 3.7 \times 10^{-7}$. Furthermore, $k_{2A} = k_{rate\ limiting}$. Converting to the corresponding free energies, substituting into eq I, and solving yield $\Delta G^{\ddagger}_0$ = 15.7 kcal mol^{-1}.

Registry No. 1, 64215-73-2; Zn^{2+}, 23713-49-7; Mg^{2+}, 22537-22-0; enolpyruvate, 118890-91-8; pyruvate, 57-60-3.

(47) Baigrie, L. M.; Cox, R. A.; Slebocka-Tilk, H.; Tencer, M.; Tidwell, T. T. *J. Am. Chem. Soc.* **1985**, *107*, 3640.
(48) Murdoch, J. R. *J. Am. Chem. Soc.* **1983**, *105*, 2660.
(49) Grunwald, E. J. *J. Am. Chem. Soc.* **1985**, *107*, 125.
(50) Chiang, Y.; Kresge, A. J.; Tang, Y. S. *J. Am. Chem. Soc.* **1984**, *106*, 460.
(51) Sander, E. G.; Jencks, W. P. *J. Am. Chem. Soc.* **1968**, *90*, 6154.
(52) Guthrie, J. P. *Can. J. Chem.* **1978**, *56*, 962.
(53) Capon, B.; Zucco, C. *J. Am. Chem. Soc.* **1982**, *104*, 7567. Capon, B.; Guo, B. Z.; Kwok, F. C.; Siddhanta, A. K.; Zucco, C. *Acc. Chem. Res.* **1988**, *21*, 135.
(54) Guthrie, J. P.; Cullimore, P. A. *Can. J. Chem.* **1979**, *57*, 240.